Article title: Phosphorylation of the exocyst subunit Exo70B2 contributes to the regulation of its function

Authors: Ooi-Kock Teh[1,2,3], Chil-Woo Lee[1,4], Franck Aniset Ditengou[5], Till Klecker[6], Giulia Furlan[1], Marco Zietz[1], Gerd Hause[7], Lennart Eschen-Lippold[1], Wolfgang Hoehenwarter[1], Justin Lee[1], Thomas Ott[5], Marco Trujillo[1]

[1]Leibniz Institute of Plant Biochemistry, Halle (Saale) 06120, Germany

[2]Present address: Institute for International Collaboration, Hokkaido University, Sapporo 060-0815, Japan

[3]Department of Biological Science, School of Science, Hokkaido University, 060-0810, Japan

[4]Present address: Korea Honey Bee Disease Institute, Gyeonggi-do, 16227, Korea

[5]Institute of Cell Biology, University of Freiburg, 79104 Freiburg, Germany

[6]Institute of Cell Biology, University of Bayreuth, 95440 Bayreuth, Germany

[7]Biozentrum, Martin-Luther-University Halle-Wittenberg, Halle (Saale) 06120, Germany

Author for correspondence: Marco Trujillo, Leibniz Institute of Plant Biochemistry, Halle (Saale) 06120, Germany, Email: mtrujillo@ipb-halle.de , phone: +49 (0) 345-5582-1720, fax: +49 (0) 345-5582-1709

Abstract

The exocyst is a conserved hetero-octameric complex mediating early tethering during exocytosis. Its Exo70 subunit plays a critical role as a spatiotemporal regulator by mediating numerous protein and lipid interactions. However, a molecular understanding of the exocyst function remains challenging. We show that Exo70B2 locates to dynamic foci at the plasma membrane and transits through a BFA-sensitive compartment, reflecting its canonical function in secretion. However, treatment with the salicylic acid (SA) defence hormone analogue Benzothiadiazole (BTH), or the immunogenic peptide flg22, induced Exo70B2 transport into the vacuole. We uncovered two ATG8-interacting motifs (AIMs) located in the C-terminal domain (C-domain) that mediate its recruitment into the vacuole. Moreover, we also show that Exo70B2 is phosphorylated near the AIMs and mimicking phosphorylation enhanced ATG8 interaction. Finally, Exo70B2 phosphonull lines were hypersensitive to BTH and more resistant to avirulent bacteria which induce SA production. Our results suggest a molecular mechanism in which phosphorylation of Exo70B2 by MPK3 functions in a feed-back system linking cellular signalling to the secretory pathway.

Introduction

The exocyst is an evolutionary conserved protein complex implicated in the tethering of secretory vesicles to the plasma membrane (PM) before SNARE-mediated membrane fusion. The first exocyst components were described in yeast as temperature sensitive mutants in which vesicles accumulated due to failed fusion to the PM (Novick et al., 1980). All subunits of the exocyst were later shown to work in a complex and to mediate exocytosis of post-Golgi vesicles (Wu and Guo, 2015). The complex was subsequently found to be conserved in plants, and the first reported mutant phenotypes supported the anticipated function in secretion (Cole et al., 2005; Wen et al., 2005). However, in contrast to all other eukaryotic organisms, the Exo70 subunit has experienced a substantial expansion into many paralogues; 23 in *Arabidopsis thaliana* (referred to as Arabidopsis) and 47 in rice (Cvrckova et al., 2012).

The secretory pathway mediates the transport of lipids and proteins to the PM. Specific conditions such as active growth and infection, engage the secretory pathway and significantly enhance its activity (Wang et al., 2005). During the immune response de-novo synthesis of a vast array of proteins is induced, including PM-localized receptors and proteins with antimicrobial activities which are delivered to the extracellular space (Gu et al., 2017). The defence hormone SA plays a key function by coordinately upregulating the secretory pathway (Wang et al., 2005; Tateda et al., 2014).

Localization of Exo70 in humans and yeast to the PM is mediated by its ability to bind phosphatidylinositol 4,5-bisphosphate (PI(4,5)P_2) (He et al., 2007a; Liu et al., 2007). Although direct membrane binding of an exocyst component has not been shown in plants, the small molecule

57 Endosidin2 (ES2) binds to Exo70A1 and inhibits its exocytosis and recycling (Zhang et al., 2016).
58 Residues contributing to ES2 binding were located in the C-domain of Exo70A1 at the C-terminus,
59 suggesting that the membrane-binding function of the C-terminal region is conserved in plants.
60 The exocyst has been shown to play a role in the immune response of both plants and animals. The
61 Sec5 subunit forms an effector complex with GTPase RalB and directly recruits and activates the
62 atypical IκB kinase family member TBK1 in human cells (Chien et al., 2006). The RalB/Sec5 complex
63 contributes to the activation of the innate immune response via TBK1 in response to virus infection.
64 In plants, a function in immunity has mainly been reported for Exo70 homologues. Mutants of
65 *Exo70B2* and *Exo70H1* are more susceptible to virulent bacterial pathogens (Pecenkova et al., 2011;
66 Stegmann et al., 2012). Moreover, Exo70B2 was shown to be required for full activation of pathogen-
67 associated molecular pattern (PAMP)-triggered immunity (PTI) (Stegmann et al., 2012). For Exo70B1,
68 the closest homologue of Exo70B2, there have been contrasting reports regarding its function in the
69 resistance against the bacterial pathogen *Pseudomonas syringae* pv *tomato* DC3000 (Stegmann et
70 al., 2012; Stegmann et al., 2013; Zhao et al., 2015).
71 Although the canonical function of the exocyst is exocytosis, it has been implicated in other
72 processes (Wu and Guo, 2015). Exo70B1 is transported into the vacuole and partially colocalizes with
73 ATG8, a ubiquitin-like protein required for the formation of autophagosomal membranes (Kulich et
74 al., 2013). Mutants of *exo70B1* also displayed reduced accumulation of anthocyanins and
75 spontaneous cell death reminiscent of autophagy-deficient mutants (Kulich et al., 2013). This has led
76 to the assumption that Exo70B1 plays a general function in autophagy. The Exo70E2 homologue is
77 recruited to autophagosomes after autophagy induction by BTH (Lin et al., 2015). However, under
78 control conditions it remained in distinct compartments. In human cells, RalB directly binds to Exo84,
79 inducing the assembly of catalytically active ULK1 and Beclin1-VPS34 complexes on the exocyst to
80 drive autophagosome formation (Bodemann et al., 2011).
81 A possible explanation for the different functions of the exocyst is that many cellular processes need
82 to be coordinated with exocyst-mediated exocytosis (Wu and Guo, 2015). Therefore, exocyst activity
83 must to be tightly coordinated to allow temporal and spatial control of its functions.
84 In mammals, the mitogen-activated protein kinase ERK1/2 phosphorylates Exo70 in response to
85 epidermal growth factor (EGF), resulting in the assembly of the exocyst complex and secretion (Ren
86 and Guo, 2012). Adding another regulatory layer, we previously showed that upon activation of PTI,
87 Exo70B2 was targeted by the E3 ligase PUB22 for degradation during the immune response
88 (Stegmann et al., 2012; Furlan et al., 2017).
89 In this study, we show that part of the cellular Exo70B2 pool is localized to the PM, and in contrast to
90 other exocyst subunits, transits through a BFA-sensitive compartment. Treatment with the SA
91 analogue BTH induces the accumulation of Exo70B2 in the microsomal membrane fraction, which
92 reflects its transport into the vacuole by autophagy. Exo70B2 can be phosphorylated by the PAMP-

93 responsive MPK3, and plants expressing a non-phosphorylatable version display enhanced
94 sensitivity to BTH, as well as increased resistance to avirulent bacteria. The enhanced interaction of
95 the Exo70B2 phosphomimic with ATG8 suggests that phosphorylation contributes to Exo70B2
96 degradation by autophagy, inhibiting its participation in exocytosis.
97

98 # Results

99 **Exo70B2 localizes to dynamic foci at the plasma membrane**

100 In an effort to gain insight into exocyst function, and in particular of the Exo70B2 subunit, we
101 characterized stable transgenic lines carrying the GFP-Exo70B2 fusion under control of the *UBQ10*
102 promoter in the *exo70B2-3* background (Grefen et al., 2010). We opted to employ the *UBQ10*
103 promoter, because lines under the control of a 1.5kbp fragment upstream of the *Exo70B2* CDS didn't
104 lead to detectable expression, similarly to what was reported by Li et al. (Li et al., 2010).
105 GFP-Exo70B2 was detected in the cytoplasm of epidermal cells in cotyledon and roots, as well as a
106 continuous cell-peripheral localization, which suggested PM localization (Figure 1A). To confirm PM
107 localization, we plasmolysed cells using mannitol. GFP-Exo70B2 was detected at the periphery and
108 in Hechtian strands of plasmolysed epidermal cells, suggesting that Exo70B2 localized to the PM
109 (Figure 1B). To support our observations, we analysed the localization in root hairs which show tip
110 growth, reasoning that GFP-Exo70B2 function would be focused to regions of high secretory activity
111 (Honkanen and Dolan, 2016). High-resolution microscopy revealed that GFP-Exo70B2 localized to
112 distinct foci at the periphery of in root hairs and the number of foci increased towards the tip where
113 secretory activity is highest. The additional analysis by variable angle epifluorescence microscopy
114 (VEAM)TIRF microscopy demonstrated that these foci are dynamic with a transient dwelling at the
115 PM (Movie S1).
116 Treatment with BFA, which inhibits endosomal recycling of PM proteins, resulted in the
117 accumulation of Exo70B2 in BFA-bodies, indicating that it transits through the *trans*-Golgi network
118 (TGN) (Figure 1C). These results are consistent with a canonical function of Exo70B2 in the secretion
119 of post-Golgi vesicles.

120 **Exo70B2 is transported into the vacuole where it colocalizes with autophagic markers**

121 We previously reported that Exo70B2 is targeted for degradation after activation of the immune
122 response by the E3 ligase PUB22 (Stegmann et al., 2012). Ubiquitination of Exo70B2 by PUB22
123 suggested that it may be targeted for degradation via the proteasome. However, its association to
124 the PM and accumulation in BFA-bodies indicated that Exo70B2 enters the endocytic, or alternate
125 degradation pathways, capable of processing membrane-associated proteins. In support of such a
126 scenario, studies in mammals have shown that exocyst participates in the activation of autophagy
127 (Bodemann et al., 2011). Moreover, Exo70B1 and Exo70E2 colocalized with the autophagy marker

128 ATG8 upon tunicamycin or BTH treatment respectively, in plants (Ichimura et al., 2000; Kulich et al.,
129 2013; Lin et al., 2015).
130 To induce autophagy we employed BTH (Yoshimoto et al., 2009; Lin et al., 2015), which is an analogue
131 of the phytohormone SA, a central component of the immune response and induces the expression
132 of hundreds of genes (Wang et al., 2005; Vlot et al., 2009). Inhibition of the vacuolar degradation by
133 Concanamycin A (ConcA), revealed basal transport of Exo70B2 into the vacuole, reflected by the
134 accumulation of punctae in the vacuole of elongated epidermal root cells, but not detectable in
135 cotyledon cells (Figure 2A). By contrast, co-treatment with BTH induced the accumulation of
136 intravacuolar punctae in both roots and cotyledons (Figure 2A). Analysis of Sec6, another subunit of
137 the exocyst, showed that BTH had a similar effect and resulted in its delivery to the vacuole (Figure
138 S1A).
139 Supporting the transport of Exo70B2 into the vacuole by autophagy, the marker proteins ATG8a and
140 NBR1 colocalized to a subpopulation of punctae after BTH/ConcA treatment (Figure 2B) with
141 Pearson's correlation coefficients of 0.48 for ATG8 and 0.4 for NBR1 (Figure 2C) (Kirkin et al., 2009;
142 Svenning et al., 2011). Moreover, ultrastructural analysis confirmed that Exo70B2 was transported
143 into the vacuole upon autophagy induction (Figure S1B).
144 To further dissect the behaviour of Exo70B2, we analysed the effect of BTH on protein levels. Analysis
145 of total protein detected by immunoblot (IB) did not show obvious changes after BTH treatment, in
146 spite of increased fluorescence intensity (Figure 2E, upper panel). Similarly, ConcA treatment, alone
147 or in combination with BTH, resulted in only minor variations of Exo70B2 in total protein extracts.
148 Because BTH treatment remobilises Exo70B2 to the vacuole, we analysed protein fractions
149 containing both soluble and microsomal proteins and lacking larger organelles such as nuclei and
150 chloroplasts. In contrast to total protein, this fraction contained non-detectable levels of Exo70B2 in
151 control samples (Figure 2E, lower panel). However, treatment with BTH and ConcA, alone or
152 combined, resulted in increased amounts of Exo70B2. Moreover, GFP cleavage, which can be
153 indicative of autophagy (Marshall et al., 2015), was observed for samples treated with ConcA, BTH
154 and ConcA.
155 This fraction was further separated by ultracentrifugation, resulting in a microsomal pellet
156 containing membrane-bound proteins, and a supernatant with soluble proteins. Comparison of
157 equivalent samples amounts showed that while Exo70B2 was present in the microsomal fraction, it
158 was not detectable as a soluble protein (Figure 2F). However, higher levels present in the total
159 protein extract, also indicate additional populations of Exo70B2 (Figure 2F). Finally, we show that
160 microsome-associated Exo70B2 increases upon BTH treatment (Figure 2G).
161 Taken together, BTH activates Exo70B2 transport into the vacuole potentially by autophagy, which
162 is reflected by the colocalization with ARG8 and the remobilization of Exo70B2 sub-pools to
163 membrane fractions.

164 **Exo70B2 is transported into the vacuole upon activation of the immune response**

165 Because we previously showed that Exo70B2 contributed to PTI (Stegmann et al., 2012), we tested
166 the impact of activating the immune response. Treatment with flg22, which is perceived by the
167 immune receptor FLS2, or ConcA alone, did not result in detectable changes (Figure 3A). However,
168 flg22/ConcA co-treatment revealed the transport of Exo70B2 into the vacuole (Figure 3A). As
169 previously shown, flg22 treatment resulted in the degradation of Exo70B2 (Figure 3B). To test
170 whether this reflected vacuolar degradation, we pre-treated seedlings with ConcA. Inhibition of the
171 vacuolar degradation reduced Exo70B2 degradation (Figure 3B).

172 Since flg22 treatment induced Exo70B2 transport into the vacuole, we wondered whether flg22
173 potentially increased autophagic flux. Treatment of seedlings with flg22, resulted in an increase of
174 NBR1 protein levels, and flg22/ConcA co-treatment further enhanced this effect (Figure S2A). In
175 accordance, NBR1 accumulated in the vacuole in response to flg22, and co-treatment with ConcA
176 resulted in both a diffuse vacuolar signal and perivacuolar punctae (Figure S2B). These results are in
177 agreement with a potential degradation of Exo70B2 by autophagy in response to the activation of
178 the immune response.

179 **Exo70B2 interacts with and is phosphorylated by MPK3 in vitro**

180 Induction of Exo70B2 transport into the vacuole by flg22 treatment prompted us to search for a link
181 to immune signalling. Exocyst subunits including Exo70B2 were reported to be significantly
182 increased in phosphoprotein-enriched fractions of Arabidopsis plants expressing the constitutively
183 active MKK5-DD variant in comparison to the kinase-inactive KR mutant: Exo70B2 by 2.28 fold (p
184 value <0.001), Exo70E1 2.35 fold (p value <0.05) and Sec5A 2.86 fold (p value <0.05) (Lassowskat et
185 al., 2014; Lee et al., 2015). FLS2 activation by flg22 induces the MKK5 branch of MAPKs, which
186 includes MPK3 or MPK6 and other downstream kinases. Because MAPK signalling, and possibly
187 autophagy, are induced during the immune response, we hypothesized that Exo70B2 may represent
188 a link between these pathways.

189 To evaluate this possibility, we first assayed the interaction with MPK3, MPK4, MPK6, MPK8 and
190 MPK11 using bimolecular fluorescence complementation (BiFC). We found that from the tested
191 MAPKs, both MPK3 and MPK11 reconstituted fluorescence when transiently coexpressed with
192 Exo70B2 (Figure 4A and Figure S3A). Although the BiFC results suggested that Exo70B2 also interacts
193 with MPK11, the lack of specific MPK11 antibodies and the typically low activity of MPK11 (Bethke et
194 al., 2012), impedes its analysis. Therefore, we decided to focus on MPK3, which was also shown to
195 phosphorylate the E3 ligase PUB22, which targets Exo70B2's (Furlan et al., 2017). Confirming the
196 interaction, endogenous MPK3 co-immunoprecipitated (IP) with Exo70B2 by anti-GFP antibodies in
197 two independent homozygous lines (T3) carrying the *UBQ10prom-GFP-Exo70B2* construct in the
198 *exo70B2-3* background (Figure 4B). The interaction was independent of flg22 treatment, suggesting
199 that both proteins constitutively associate under the tested conditions. In vitro pull-down

200 experiments of bacterially expressed Exo70B2 and MPK3 showed that both proteins interacted
201 directly, while MPK6 displayed only a weak interaction (Figure 4C).
202 Interaction between Exo70B2 and MPK3 opened the possibility that Exo70B2 is a substrate of MPK3.
203 To test this, we carried out in vitro phosphorylation assays using purified recombinant MPK3, MPK4,
204 MPK6 and MPK11. Consistent with the direct interaction, Exo70B2 was readily trans-phosphorylated
205 by MPK3 but not by MPK4 or MPK6 (Figure 4D). In the case of MPK11, kinase activity of recombinant
206 MPK11 is typically low in our hands, and consequently, no phosphorylation of Exo70B2 was
207 detectable.
208 Recombinant Exo70B2 phosphorylated by MPK3 was next analysed by LC-MS/MS to determine the
209 phosphorylation sites. We identified two residues, namely S554 and S567, both of which are located
210 in the C-domain at the C-terminal portion of the protein (Figure 4E and Figure S3B). Both residues
211 are followed by a proline, and thus represent typical MAPK phosphorylation motifs. No
212 phosphopeptides were identified in controls without kinase. To confirm that the phosphorylation
213 also takes place in vivo, we immunopurified GFP-Exo70B2 from transgenic seedlings treated with
214 flg22 for 30 and 140 min and analysed samples by LC-MS/MS. Both phosphorylations in residues
215 S554 and S567 could be identified, indicating that phosphorylation also takes place in vivo, while no
216 phosphorylation was detected in non-treated samples (Figure S3C and Table S2). A sequence
217 alignment between Exo70 homologues of the identified sites indicates that these residues are not
218 conserved, suggesting a specialized regulatory function in Exo70B2 (Figure S3D).
219 **Exo70B2 interaction with ATG8 through AIMs is increased in phosphomimic variant**
220 Sequence analyses have predicted an over proportional presence of ATG8-interaction motifs (AIMs)
221 in the Arabidopsis Exo70 family (Cvrckova and Zarsky, 2013; Tzfadia and Galili, 2013). We identified
222 two putative AIMs located in the C-domain of Exo70B2: AIM1 508-DGPYPKL and AIM2 522-SQFDEV
223 (Figure 5A).
224 We first tested the interaction by coexpressing Exo70B2 with ATG8f, which resulted in fluorescence
225 complementation in a BiFC assay (Figure 5B and Figure S4A). To confirm that the interaction was
226 mediated by the AIMs, we generated mutants in which we replaced YPKL (AIM1) and FDEV (AIM2)
227 by APKA and ADEA, respectively. Mutation of single AIMs significantly compromised
228 complementation in comparison to WT Exo70B2, and was mostly abrogated in the ΔAIM1/AIM2
229 double mutant (Figure 5B). To further characterize the interaction, we carried out in vitro pull-down
230 assays with purified recombinant proteins. MBP-Exo70B2 was able to co-purify His-ATG8f, indicating
231 that the proteins interact directly (Figure 5C).
232 The presence of AIMs in Exo70B2 suggested that they mediate its transport into the vacuole via
233 autophagy. We transiently coexpressed Exo70B2 WT and the ΔAIM1/AIM2 variant with ATG8a and
234 tested delivery into the vacuole in the presence of BTH and ConcA. As previously shown, Exo70B2
235 was autophagocytosed together with ATG8 (Figure 5D). However, the ΔAIM1/AIM2 mutant

236 remained outside of the vacuole, indicating that autophagy of Exo70B2 requires the presence of
237 AIMs.
238 In contrast to AIM1, which is located in a highly variable region of the Arabidopsis Exo70 family, AIM2
239 is present in 65% of the Arabidopsis Exo70 homologues, as well as conserved in *Saccharomyces*
240 *cerevisiae* Exo70 (Figure S4B). The conservation of the second AIM in the yeast Exo70, opened the
241 possibility that the interaction with ATG8 and its transport into the vacuole, represent an ancestral
242 function. We therefore generated a yeast strain expressing an Exo70-FLAG fusion protein from a
243 genomic insertion and transformed these cells with a plasmid carrying GFP-ATG8. Under nutrient
244 replete conditions Exo70 interacted with ATG8 (Figure S4C), and the interaction was markedly
245 increased after 1h nitrogen (N) deprivation (Figure S4C). These results show that the interaction
246 between Exo70 and ATG8 is conserved across kingdoms and that analogously to plants, the
247 interaction with ATG8 uncovers a link to autophagy.
248 Notably, the identified MAPK-mediated phosphorylation sites are located in the vicinity of the AIMs,
249 suggesting a potential role in their regulation (Figure 5A). To test whether phosphorylation had an
250 impact on the interaction with ATG8, we also tested the non-phosphorylatable (S554/567A) and
251 phospho-mimetic (S554/567D) variants of Exo70B2. Coexpression of ATG8 with S554/567A
252 displayed a significantly decreased YFP complementation, when compared to S554/567D (Figure 5E
253 and Figure S5A), suggesting that phosphorylation of serines increases Exo70B2's ability to interact
254 with ATG8. We further confirmed these results by in vitro pull-down assays. In comparison to the
255 S554/567A Exo70B2, ATG8 was co-precipitated more efficiently by the S554/567D phosphomimetic
256 variant, suggesting a stronger interaction (Figure 5F). However, both mutant variants were still
257 delivered to the vacuole (Figure S5B).
258 In order to obtain some insight into the possible mechanism by which phosphorylation of S554 and
259 S567 influences ATG8 binding to the AIMs, we generated a structural model of Exo70B2's C-domain.
260 Various crystal structures are available, including the Arabidopsis Exo70A1 homologue (Zhang et al.,
261 2016). However, the model with the highest confidence was obtained using the yeast Exo70
262 structure (pdb 2pfv; Figure S6A) (Moore et al., 2007). Serine 554 is predicted to be positioned directly
263 opposite and in close proximity to AIM1, opening the possibility that phosphorylation influences
264 ATG8 binding by generating a negative charge that enhances affinity (Figure S6B). Serine 567, on the
265 other hand, is positioned on the side opposite to the AIM2 docking surface, suggesting an allosteric
266 effect when phosphorylated.
267 Together, we show that Exo70B2 autophagy requires its AIM motifs, and that phosphorylation at
268 S554 and S567 may control ATG8 interaction.
269

270 **Expression of Exo70B2 phosphonull variant enhances sensitivity to BTH and resistance to**
271 **avirulent bacteria**
272 Our results show that Exo70B2 is a substrate of autophagy, as reflected by the BTH-induced
273 accumulation in the microsomal fraction. Moreover, activating the immune response by flg22
274 treatment induced the transport of Exo70B2 into the vacuole.
275 In order to investigate the function of Exo70B2 phosphorylation, we scored the impact of BTH on
276 seedling root growth of *exo70* mutants, and lines complemented with WT, phosphonull or
277 phosphomimetic Exo70B2 variants (Figure S7A and Figure S7B). BTH had little to no effect on root
278 growth of Col-0 plants when compared with controls under the used conditions (Figure 6A and Table
279 S2). Similarly, no major changes were observed for the other lines, with the exception of *exo70B2-3*
280 plants complemented with WT Exo70B2 and the S554/567A phosphonull variant (Figure 6A and
281 Table S2). Both transgenic lines expressing the WT and S554/567A Exo70B2 showed root growth
282 inhibition in the presence of BTH. Of note, the S554/567A phosphonull mutant was significantly
283 more sensitive than WT Exo70B2 expressing lines, displaying growth arrest after transplanting them
284 onto BTH-containing media. By contrast, the S554/567D phosphomimetic variant showed no
285 significant difference to the control (Figure 6A and Table S2). To compare the response to BTH we
286 also tested the accumulation of PR1, a small secreted protein with antimicrobial activities. In
287 agreement with the effect on root growth inhibition, PR1 accumulated at much higher levels in
288 seedlings expressing the S554/567A phosphonull mutant after BTH treatment (Figure 6B).
289 Because BTH is an analogue of SA, a central defence hormone, these observations suggested that
290 phosphorylation states of Exo70B2 may also affect plant immune responses. We subsequently
291 carried out pathogen infection assays using the virulent *Pseudomonas syringae* pv. *tomato* DC3000
292 (*Pst*), as well as an avirulent *Pst* strain expressing the AvrRPS4 effector, which is recognized in
293 Arabidopsis and activates effector-triggered immunity (ETI). As previously reported, *exo70B2-3* is
294 more susceptible to the virulent *Pst* when compared to the WT Col-0 (Figure 6C). Re-introducing the
295 *GFP-Exo70B2* complemented the enhanced susceptibility back to WT levels (Figure 6C). The
296 S554/567A and S554/567D mutants however, also complemented the phenotype and displayed no
297 differences to the WT. Nevertheless, lines transformed with the ΔC construct displayed *exo70B2-3*
298 levels of susceptibility, indicating that the C-domain is required for Exo70B2 function in resistance to
299 *Pst*.
300 Because the S554/567A variant conferred BTH hypersensitivity, we reasoned that Exo70B2 may also
301 function in responses that induce the SA pathway. During ETI, plants trigger the hypersensitive
302 response, which is a robust immune reaction characterized by programmed cell-death and the
303 concomitant accumulation of high levels of SA (Jones and Dangl, 2006). In agreement with the
304 enhanced sensitivity to BTH, growth of *Pst-AvrRPS4* was strongly reduced in plants expressing the
305 S554/567A variant (Figure 6D). No significant differences were observed for the other lines.

306 These results demonstrate that mutating residues S554 and S567 to non-phosphorylatable alanines,
307 renders plants more sensitive to BTH and results in an increased resistance during ETI. Hence,
308 phosphorylation of Exo70B2 is potentially required to regulate processes triggered by BTH or SA.
309

310 # Discussion

311 **Exo70B2 and vesicle tethering**

312 The canonical function of the exocyst complex is exocytosis by mediating early tethering of post-
313 Golgi vesicles before SNARE-mediated membrane fusion. Recent studies indicate that the plant
314 exocyst can mediate polarity of the ATP-binding cassette transporter PEN3 at the PM (Mao et al.,
315 2016), and coordinate the transport of CASP1 to specific regions in the PM through the Exo70A1
316 subunit (Kalmbach et al., 2017). In line with these observations, our results indicate that Exo70B2 also
317 locates to the PM in dynamic foci. Furthermore, the accumulation in BFA-compartments indicates
318 that Exo70B2 transits through the TGN. This trait is, to the best of our knowledge, exclusive to
319 Exo70B2, and suggests that it may have adopted unique features. The localization to the PM and
320 accumulation in BFA-bodies reflect the canonical function of Exo70B2 in post-Golgi vesicle transport
321 in secretion (Figure 1B, Figure 1C and Figure 7).

322 **Additional roles of Exo70B2**

323 It has become clear in recent years, that the exocyst is additionally involved in autophagy
324 (Bodemann et al., 2011), but its exact roles still need to be defined. Several links have recently been
325 reported connecting the exocyst, and more specifically its Exo70 subunits, to autophagy in plants.
326 Here, we reveal that Exo70B2 possesses two AIMs located in the C-domain that mediate its transport
327 into the vacuole by directly interacting with ATG8 for autophagy (Figure 4D). Similar to observations
328 by Lin and colleagues (2015), we show that BTH induces the colocalization of Exo70B2 punctae with
329 ATG8 and NBR1 (Figure 2B), and additionally, that flg22 treatment also results in Exo70B2 transport
330 into the vacuole for degradation.

331 Moreover, we identify two phosphorylation sites located in the C-domain of Exo70B2. The C-domain
332 of Exo70 subunits harbours the surface that mediate the interaction with phospholipids (He et al.,
333 2007a; Mei et al., 2018). A conserved function of the C-domain in plants was indirectly demonstrated
334 for Exo70A1, which is targeted by the small molecule Endosidin2. Binding of Endosidin2 to a pocket
335 within the C-domain inhibits Exo70A1 function (Zhang et al., 2016).

336 There are two possible mutually nonexclusive scenarios by which phosphorylation of Exo70B2 may
337 modulate its function. First, phosphorylation regulates Exo70B2 binding to the PM, therefore the
338 phosphonull variant may be locked in its canonical secretory function. Identified sites are located in
339 the C-domain, which mediates the interaction of Exo70 orthologues with PM phosphoinositides
340 through ionic interactions (He et al., 2007a; Liu et al., 2007). Exo70B2 is predicted to possess polybasic

341 regions in the C-domain which could mediate interaction with phospholipids (Figure S9A) (Liu et al.,
342 2007; Zhao et al., 2013; Pleskot et al., 2015). Phosphorylation sites (S554 and S567) are placed
343 adjoining to the last stretch of a basic ridge (Figure S9A), opening the possibility that introduction of
344 negative charges by phosphorylation modulates phospholipid binding.
345 In a second scenario, enhanced interaction with ATG8 may contribute in redirecting Exo70B2 into
346 the autophagic pathway (Figure 7). S554 is predicted to be in close proximity to AIM1, opening the
347 possibility that phosphorylation controls the interaction with ATG8 by generating a negatively-
348 charged patch, known to increase ATG8 binding (Figure S6B) (Noda et al., 2010).
349 However, the mutant variant S554/567A was not significantly affected in its transport into the
350 vacuole, indicating that phosphorylation may contribute to autophagy but is dispensable (Figure
351 S5B). A possible reason for this observation is that Exo70B2 is delivered to the vacuole by an
352 alternative pathway. Because Exo70B2 cycles between the PM and TGN, it may additionally enter the
353 canonical endocytic degradation pathway. Indeed, a subpopulation of punctae did not colocalize
354 with ATG8 (Figure 2B). In line with these observations, colocalization of Exo70E2 and ATG8e was
355 significantly increased after longer BTH and ConcA treatments (Lin et al., 2015).
356 AIMs are typically found in autophagic receptors, such as NBR1, and act as tethers by additionally
357 binding ubiquitinated substrates to mediate the association to autophagosomes, in a process
358 termed selective autophagy (Kirkin et al., 2009; Svenning et al., 2011). The presence of AIMs in
359 Exo70B2 suggests that it may additionally drive the transport of the associated exocyst complex.
360 Supporting such a scenario, Exo70B2 binds to the core subunit Exo84 (Stegmann et al., 2012), and
361 BTH treatment induced the accumulation of autophagosome-like compartments of the Sec6 subunit
362 (Figure S1A).
363 Exo70B1 colocalization with ATG8 and the development of spontaneous cell death lesions before
364 flowering are reminiscent of autophagy defective mutants. This has led to the hypothesis that it plays
365 a general function in autophagy. However, a recent study revealed that *exo70B1*'s cell death
366 phenotype is dependent on the truncated immune sensor TN2 (Zhao et al., 2015), putting into
367 question the relation of Exo70B1's proposed general role in autophagy (Kulich et al., 2013). Other
368 Arabidopsis *exo70* mutants also do not display typical autophagy deficiency phenotypes (Zhao et al.,
369 2015). Therefore, Exo70 subunits in Arabidopsis are likely to act downstream of autophagy
370 activation, where they are substrates and/or may mediate selective autophagy.
371 Interaction of yeast ATG8 and Exo70 indicates a across-kingdoms conservation, suggesting that this
372 represents an ancestral function. Indeed, silencing of the human Exo70 did inhibit the formation of
373 autophagosomes (Bodemann et al., 2011). Supporting a conserved role in autophagy, disruption of
374 Arabidopsis and *Brassica napus* Exo70A1 function inhibits the formation of secretory vesicles and
375 multivesicular bodies (MVBs) at zones of pollen reception in the stigma PM (Samuel et al., 2009;
376 Safavian et al., 2015). Similarly, for self-incompatible pollinations, secretory vesicles and MVBs are

377 absent from the PM of stigmatic papillae, and autophagy appeared to be induced to redirect vesicles
378 and MVBs to the vacuole (Safavian and Goring, 2013).

379 **Exo70B2 and Immunity**

380 The secretory pathway is intimately engaged in the immune response to pathogens. It mediates the
381 delivery of both plasma membrane inherent proteins such as immune receptors and ABC-
382 transporters such as FLS2 and PEN3, respectively (Dormann et al., 2014), as well as soluble proteins
383 that are secreted into the apoplast such as PR1 (Kalde et al., 2007). As a component of the secretory
384 machinery, several lines of evidence indicate that the exocyst plays a key role in plant immunity
385 (Pecenkova et al., 2011; Stegmann et al., 2012; Ostertag et al., 2013; Stegmann et al., 2013; Fujisaki et
386 al., 2015; Zhao et al., 2015), as well as in the innate immune system of mammals (Chien et al., 2006;
387 Ishikawa et al., 2009).

388 Phosphorylation of Exo70B2 by MAPKs may act as a direct feed-back system to regulate secretory
389 activity by acting as a rheostat to surveil cellular homeostasis. SA accumulation, or treatment with its
390 analogue BTH, results in a massive increase of secretory activity (Wang et al., 2005; Nagashima et al.,
391 2014). Importantly, upregulation by SA or BTH poses severe strains on the secretory pathway,
392 causing cellular stress and activating responses that include the unfolded protein response to
393 maintain homeostasis (Wang et al., 2005; Nagashima et al., 2014; Angelos et al., 2017). Such
394 responses are conserved across kingdoms and are required to maintain and execute immune
395 responses (Zhang et al., 2015; Grootjans et al., 2016). Thus, redirection of Exo70B2 into the vacuole
396 for degradation may contribute to the downregulation of the secretory activity (Angelos et al., 2017).
397 Accordingly, plants expressing the Exo70B2 S554/567A phosphonull variant were significantly more
398 sensitive to BTH (Figure 6A) and more resistant to the avirulent *Pst* strain that triggered ETI (Figure
399 6D).

400 A caveat to this interpretation is that *exo70b2-3* complemented with a WT Exo70B2 also conferred
401 BTH hypersensitivity, albeit significantly weaker than the S554/567A Exo70B2 variant. This
402 observation possibly reflects an altered stoichiometry of Exo70B2 to kinases such as MPK3, leading
403 to increased levels of non-phosphorylated Exo70B2 species that result in a phosphonull-like
404 phenotype. Moreover, the inability of the phosphonull variant, but not of the phosphomimetic
405 variant, to restrict the growth arrest response induced by BTH, underscores the importance of S554
406 and S567 phosphorylation.

407 Exo70B2 contributes to PTI (Figure 6C) (Stegmann et al., 2012), but mutation of the phosphorylation
408 sites did not affect resistance to virulent bacteria suggesting mutant variants are still active.
409 However, the C-terminus is indispensable for functionality since ΔC mutants did not complement
410 the *exo70B2-3* phenotype (Figure 6C).

411 We previously showed that Exo70B2 is targeted by the E3 ubiquitin ligase PUB22, and is rapidly
412 degraded in response to flg22 treatment (Stegmann et al., 2012). Here we show that Exo70B2 is

413 transported to the vacuole for degradation also after flg22 elicitation. While PUB22 mediates its own
414 degradation through the proteasome (Furlan et al., 2017), it probably contributes to Exo70B2
415 degradation by modification with alternative types of ubiquitin chains. Lys63-linked chains are
416 required for the degradation of membrane proteins (Leitner et al., 2012; Martins et al., 2015). This is
417 supported by studies showing that PUB12 and PUB13 mediate the degradation of membrane
418 proteins FLS2, BRI1, CERK1 and ABI1 (Lu et al., 2011; Kong et al., 2015; Liao et al., 2017; Zhou et al.,
419 2018).

420 **Conclusion**

421 Together, our results suggest that Exo70B2 represents an intersection point in which immune
422 signalling, secretory and autophagic pathways meet. It participates in two distinct cellular pathways,
423 namely TGN-PM trafficking and autophagy. Our observations suggest that Exo70B2 phosphorylation
424 may contribute to its redirection from TGN-PM trafficking into the autophagic pathway, which is
425 required to control enhanced secretory activity induced by BTH and during ETI (Figure 7).

426

427 # Materials and Methods

428 **Plant materials and growth conditions**

429 Arabidopsis thaliana (Col-0 accession) was used throughout this study. Seeds were surface sterilized
430 and germinated on 1/2 Murashige Skoog media (pH 5.7) supplemented with 0.25% sucrose and 0.7%
431 agar. Arabidopsis mutants *exo70b2-3* (GK726G07), *exo70b1-1* (GK114C03) (Stegmann et al., 2012) and
432 *atg7-2* (GK-655B06) (Hofius et al., 2009) were previously described. All plants used for imaging were
433 4 day-old seedlings germinated under long day conditions (8h dark, 16 h light). Protoplasts were
434 isolated from 5-week-old plants as described before (He et al., 2007b).

435 **Pathogen Infection assays**

436 For bacterial growth experiments, six-week old plants were spray inoculated with a solution of $5x10^8$
437 c.f.u./ml *Pseudomonas syringae* pv. *tomato* DC3000 (*Pst*) as previously described (Zipfel et al., 2004).
438 Bacterial growth was measured 3 days after inoculation. For ETI, leaves were pressure-infiltrated with
439 a solution of *Pst-AvrRPS4* $O.D._{600}$ 0.001, and bacterial growth was assessed 3 days after inoculation.

440 **Protein purification and in vitro pull down**

441 Recombinant MBP-Exo70B2, GST-MPK3 and GST-MPK6 were described previously (Stegmann et al.,
442 2012). To generate recombinant His-ATG8f, coding sequence of ATG8f was cloned into pDEST17 by
443 LR reaction. For in vitro pull-down, recombinant proteins were expressed in *Escherichia coli* after
444 induction by 0.3mM at 28°C for 3-4h. To extract recombinant proteins, *E. coli* pellets from 50ml
445 cultures were sonicated in 10ml column buffer (20mM Tris-HCl pH7.4, 200mM NaCl, 1mM EDTA, 1mM
446 DTT, 1mM PMSF, 0.5% v/v Triton X-100) and incubated at 4°C for 30 min. Extracted recombinant
447 proteins were immobilized on either amylose or glutathione agarose resins. Thereafter, recombinant
448 proteins of interacting candidates were added and incubated at room temperature for 1 h before
449 washing, elution and analysed by immunoblotting.

450 **In vitro phosphorylation assay**

451 In vitro phosphorylation assays were performed in kinase buffer (20mM Hepes pH 7.5, 15mM MgCl2,
452 5mM EGTA, 1mM DTT, 0.1mM ATP, 2µCi [gamma-32P]ATP) using recombinant full length MBP-
453 Exo70B2 and active GST-MPK3, GST-MPK4 and GST-MPK11 or non-tagged MPK6 (preactivation was
454 performed using constitutively active PcMKK5-DD) (Lee et al., 2004). Samples were incubated for 30
455 min at 37 °C; reactions were stopped by addition of SDS-PAGE sample buffer and separated by 10 %
456 SDS-PAGE. Gels were stained with Coomassie Brilliant Blue and analyzed by autoradiography.

457 **Protein extraction and Immunoblot**

458 To extract total proteins, 250mg fresh weight plant material was ground in liquid nitrogen to a fine
459 powder and 2x volume buffer (10mM HEPES/KOH pH 7.5, 13.7% w/v sucrose, 5% glycerol and
460 protease inhibitor cocktail) was added and ground to homogeneity. To obtain S10, S100 and P100
461 fractions, total proteins were centrifuged either for 5 min at 10k G (resulting supernatant is S10) or

462 30 min at 100k G (resulting supernatant and pellet are S100 and P100 fractions, respectively). Before
463 resolving on SDS-PAGE, 1x volume of 2x Laemmli sample buffer was added to the protein and
464 denatured at 68°C for 10min.

465 **Root growth inhibition assays**

466 To monitor impact of BTH on Arabidopsis root growth, 4-day old seedlings were transferred to 1/2
467 Murashige Skoog media (0.25% sucrose, pH 5.7) supplemented with 100mM BTH and incubated
468 vertically under short day conditions (8h light/16h dark). Primary root length was measured after 7
469 days.

470 **Life-imaging and Inhibitor treatment**

471 All treatments were performed in 1/2 MS liquid media unless otherwise stated. To assay the increase
472 in GFP-Exo70B2 fluorescence intensity, four-day old seedlings were incubated overnight in 100µM
473 BTH. Quantification of increased fluorescence intensity (FI) signal was performed using Fiji ImageJ as
474 described previously (McCloy et al., 2014). To visualize BFA compartments, seedlings were pre-
475 stained with 5µM FM4-64 for 5min in dark followed by incubation in 50µM BFA for 45min. To quantify
476 changes in Exo70B2 protein levels, seedlings were incubated overnight in 0.1% DMSO, 100µM BTH,
477 1µM ConcA, 50µM MG132 and 3h in 50µM CHX as well as indicated combinations. To visualize
478 increased GFP-Exo70B2 and NBR1 levels, seven to ten-day old seedlings were treated for 3h with
479 1µM ConcA, 1h 1µM flg22 or in combination.

480 Subcellular localization GFP-Exo70B2 was visualized using the Zeiss LSM780n and LSM880 Airyscan
481 laser scanning confocal microscope for high resolution images. GFP was exited using the 488 nm
482 laser in conjunction with a 505-550 band-pass.

483 For Variable angle epifluorescence microscopy (VAEM), root hairs of Arabidopsis seedlings were
484 imaged on a FEI More inverted wide field microscope (FEI, Germany) microscope using a 100 × 1.4
485 NA oil immersion objective. GFP was excited using a 488 nm solid-state laser diode. Fluorescence
486 emission was collected with an EM-CCD camera with bandwidth filters ranging from 495–550 nm
487 and fluorescence was collected with an acquisition time of 135 ms. Throughout image acquisition
488 the microscope was operated in the 'TIRF' mode for vesicles in the evanescent field (the contact area
489 between the root hair tip and the glass coverslip).

490 **Quantitative BiFC**

491 Five hundred µl of protoplasts from Col-0 or *exo70b2-3* plants were co-transformed with *pSPYNE-*
492 *ATG8F* (10 µg) and either *pSPYCE-Exo70B2* (13µg), *pSPYCE-Exo70B2AA* (13µg), *pSPYCE-Exo70B2DD*
493 (13µg), *pSPYCE-Exo70B2AIM1* (13µg), *pSPYCE-Exo70B2AIM2* (13µg), *pSPYCE-Exo70B2AIM1/2* (13µg) or
494 empty *pSPYCE* vector (13µg). *mCherry* (7.2µg) was also co-transformed as an expression marker.
495 Transformed protoplasts were incubated at room temperature for 14-16 h before CLSM imaging.
496 Thirty images (with 25-40 transformed protoplast per image) were taken for each transformation

event and used for quantification. The percentage of transformed protoplast (as indicated by mCherry expression) that showed YFP complementation was scored manually.

Accession numbers

Sequence data from this article can be found in the Arabidopsis Genome Initiative under the following accession numbers: Exo70B2 (At1g07000); Exo70B1 (At5g58430); NBR1 (At4g24690); ATG8A (At4g21980); ATG8F (At4g16520); MPK3 (At3g45640); MPK4 (At4g01370); MPK6 (At2g43790); MPK11 (At1g01560).

Acknowledgments

The authors thank Deborah Gasperini for critical reading of the manuscript and all the members of the Trujillo laboratory for fruitful discussions and valuable comments. We thank Theresa Binder for help with the generation of the yeast strain. We are grateful for materials kindly provided by Viktor Zarsky *SEC6prom:SEC6-GFP* lines, Daniel Hofius anti-NBR1, Ken Shirasu anti-HSP90, Erika Isono *pENTR-ATG8f*, and to Steingrim Svenning and Terje Johansen for *pENTR-NBR1*.

List of Author contributions

O.K.T., C.W.L., P.M., T.K., G.F., M.Z., G.H., L.E.L., F.D. conducted experiments; T.O., W.H., J.L., M.T. designed experiments and analysed the data; M.T. wrote the paper

Funding information

This research was funded by the Leibniz association and the state of Saxony-Anhalt (O.K.T., G.F., P.M, W.H., M.Z. and M.T.), DFG SPP1212 (C.W.L.) and DFG SFB648 (J.L.).

Corresponding author email

mtrujillo@ipb-halle.de

Figure legends

Figure 1. Exo70B2 transits through the trans-Golgi network and localizes to the plasma membrane

(A) Confocal laser-scanning microscopy images of four-day old homozygous transgenic seedlings expressing GFP-Exo70B2 under the control of the constitutive promoter *UBQ10* in the *exo70b2-3* background. Shown are epidermal cells of cotyledons (top left) and roots (right) and transverse section of root (right bottom). Size bars represent 20µm (cotyledons) and 10µm (roots). **(B)**

530 *UBQ10pro:GFP-Exo70B2/exo70b2-3* transgenic seedlings were incubated in 0.8M mannitol for 40
531 mins before analysed by CLSM. Plasmolysis is shown by the shrinking protoplasts. GFP-EXO70B2 is
532 visible on the Hechtian strands indicated by arrowheads. Scale bar 10µm. **(C)** High-resolution
533 microscopy pictures of *UBQ10pro:GFP-Exo70B2/exo70b2-3* transgenic seedling root hairs. Three
534 optical sections are shown from root hair shaft to tip. Scale bar 10µm, V denotes vacuole **(D)**
535 *UBQ10pro:GFP-Exo70B2/exo70b2-3* transgenic seedlings were stained with 5µM FM4-64 for 5 mins
536 and subsequently incubated in 50µM BFA for 45 mins at room temperature. Scale bar 5µm.
537
538 **Figure 2. Exo70B2 is transported into the vacuole and colocalizes with autophagic markers**
539 **(A)** GFP-EXO70B2 is localised to autophagic body-like compartment after BTH and ConcA treatment.
540 *UBQ10prom:GFP-Exo70B2/exo70b2-3* seedlings were treated o/n with either 0.1% DMSO, 1µM ConcA,
541 100µM BTH or 1µM ConcA + 100µM BTH. Confocal images of the same tissue were taken with
542 identical imaging settings. Scale bars for cotyledon and root tissues are 20µm and 10µm respectively.
543 **(B)** GFP-Exo70B2 colocalizes with autophagosome markers ATG8a and NBR1. Double transgenic
544 lines carrying *UBQ10prom:GFP-Exo70B2* and *UBQ10prom:RFP-ATG8A* or *UBQ10prom:RFP-NBR1* were
545 treated overnight with 1µM ConcA + 100µM BTH before CLSM analysis. Scale bar 10µm. **(C)** Co-
546 localisation analysis for GFP-Exo70B2 with mCherry-ARG8 or mcherry-NBR1. Data points represent
547 the technical replicates of 2 independent experiments. Boxplots show median and inter quantile
548 range (IQR), outliers (> 1.5 times IQR) are shown as circles. **(D)** *UBQ10pro:GFP-Exo70B2/exo70b2-3*
549 transgenic seedlings were treated with 0.1% DMSO (control), 100µM BTH overnight (o/n), 1µM
550 ConcA o/n and indicated combinations and 50µM MG132. Samples from the same experiment were
551 aliquoted, and total protein (detergent-solubilized) or soluble and microsomal fraction (supernatant
552 from centrifugation step 5' at 12k rcf) were resolved by PAGE and analysed by IB using anti-GFP
553 antibodies (shown are two cropped sections of the same blot). Equal loading is shown by CBB
554 staining. Similar results were obtained in three biological replicates. **(E)** Total protein, soluble and
555 microsomal fractions from *UBQ10pro:GFP-Exo70B2/exo70b2-3* transgenic seedlings were resolved by
556 PAGE and analysed by IB using the indicated antibodies. Shown are equivalent protein amounts from
557 different fractions. Plasma membrane intrinsic protein2 (PIP2) and heat shock protein 90 (HSP90)
558 were used as markers for microsomal and soluble fractions, respectively. **(F)** Soluble and microsomal
559 fractions of *UBQ10pro:GFP-Exo70B2/exo70b2-3* seedlings were analysed by IB after 100µM BTH o/n
560 treatment. (F and G) Experiments were repeated with similar results.
561
562 **Figure 3. Exo70B2 is degraded during the immune response via the vacuole**
563 **(A)** *UBQ10prom:GFP-Exo70B2/exo70b2-3* seedlings were treated with 1µM flg22 (1h), 1µM ConcA (2h)
564 or 1µM flg22 (1h) + 1µM ConcA (2h) and subsequently stained for 5 mins in 5µM FM4-64. Arrowheads

565 indicate vacuolar GFP-Exo70B2. Scale bar 5µm. **(B)** Two weeks old *UBQ10prom:GFP-*
566 *Exo70B2/exo70b2-3* seedlings were treated with 1µM flg22 for the indicated times. Samples were
567 mock treated (control) or 1µM ConcA was added 1h before elicitation with flg22. Total protein
568 fractions were analysed by IB using the indicated antibody (shown are two cropped sections of the
569 same blot).
570
571 **Figure 4. EXO70B2 is phosphorylated at residues S554 and S567.**
572 **(A)** Interaction between Exo70B2 and MPK3 detected by BiFC in Arabidopsis protoplasts. nYFP-
573 MPK3, nYFP-MPK6 or nYFP-MPK11 were coexpressed with cYFP-Exo70B2 as indicated. Free mCherry
574 was coexpressed to label the cytoplasm and nucleus. Scale bar 50µm. Experiment was repeated with
575 similar results. **(B)** Transgenic seedlings carrying *UBQ10prom:GFP-Exo70B2* were treated with 1µM
576 flg22 for 20min and the S10 protein fraction (input) was subjected to IP with anti-GFP beads.
577 Endogenous coimmunoprecipitated MPK3 was detected with MPK3-antibodies. **(C)** MBP-Exo70B2
578 pull-down assay using purified GST-MPK3 and GST-MPK6 on glutathione agarose beads as baits.
579 White arrows indicate autophosphorylated kinases **(D)** GST- Exo70B2 was incubated alone or with
580 activated GST-MPK3, GST-MPK4 and untagged MPK6 (white arrowheads). MPK11 could not be
581 activated by MKK5. Phosphorylation was visualized with ProQ Diamond stain. **(E)** Cartoon depicting
582 the localization of phosphorylated sites in Exo70B2 identified by LC-MS/MS from in vitro
583 phosphorylation assays with GST-MPK3 and in vivo from GFP-Exo70B2 immunopurified from
584 transgenic lines treated with flg22.
585
586 **Figure 5. Exo70B2 interacts with ATG8 via C-terminal AIMs**
587 **(A)** Cartoon depicting the localization and sequences of ATG8-interacting motifs (AIMs) highlighted
588 in violet. Phosphorylation sites are highlighted in red. **(B)** BiFC of coexpressed nYFP-ATG8F and
589 either cYFP-Exo70B2 (WT) or mutant variants cYFP-Exo70B2-ΔAIM1 (ΔAIM1), cYFP-Exo70B2-ΔAIM2
590 (ΔAIM2), cYFP-Exo70B2-ΔAIM1/AIM2 (ΔAIM1/2) or empty pSPYCE. Conctructs were transiently
591 coexpressed in Arabidopsis mesophyll protoplasts. mCherry was transformed as a marker for
592 transformation. Boxplots show median and inter quantile range (IQR), outliers (> 1.5 times IQR) are
593 shown as circles. Percentages of fluorescence complementation obtained from 30 independent
594 images, each with 25-40 transformed protoplasts. Total protoplasts scored for WT, ΔAIM1, ΔAIM2,
595 ΔAIM1/2 and empty vector were 723, 754, 708, 683 and 542, respectively. The experiment was
596 repeated with similar results. **(C)** Pull-down (PD) assay with recombinant His-ATG8f co-purified using
597 MBP-Exo70B2 on amylose agarose beads. Asterisk indicates MBP-Exo70B2. **(D)** Transport into the
598 vacuole was tested by coexpressing ATG8a and Exo70B2 or Exo70B2-ΔAIM1/2 transiently in
599 Arabidopsis mesophyll protoplasts form *exo70b2-3* plants. To visualize GFP-Exo70B2 transported

600 into the vacuole, protoplasts were treated with 1µM ConcA + 100µM BTH at room temperature for
601 14h before CLSM imaging. Scale bar 10 µm. **(E)** BiFC of coexpressed nYFP-ATG8F and either cYFP-
602 Exo70B2 S554/567A (AA), S554/567D (DD) or empty vector were transiently coexpressed in
603 Arabidopsis mesophyll protoplasts. mCherry was used as a transformation marker. Percentage of
604 fluorescence complementation was evaluated as in **(B)**. Total protoplasts scored for Exo70B2 WT, AA,
605 DD and empty vector were 1283, 695, 1325 and 1302, respectively. The experiment was repeated
606 with similar results. **(F)** Pull-down assay using recombinant His-ATG8F co-purified with S554/567A
607 (AA) or S554/567D (DD) MBP-Exo70B2 on amylose agarose beads. Asterisk indicates MBP-Exo70B2.
608
609 **Figure 6. Plants expressing Exo70B2 phosphonull variant are more sensitive to BTH and**
610 **resistant to avirulent bacteria**
611 **(A)** Primary root lengths of *UBQ10pro:GFP-Exo70B2/exo70b2-3* transgenic seedlings expressing GFP-
612 Exo70B2 WT, S554/567A (AA), S554/567D (DD) and ΔC-domain (ΔC) measured seven days after
613 transplanting onto media +/-100µM BTH. Boxplots show median and IQR, outliers (> 1.5 times IQR)
614 are shown as circles. Values of a representative experiment. Asterisk indicate statistically significant
615 differences between control and BTH treatment (One-Way ANOVA and Tukey post hoc test, $p < 0.05$).
616 Experiment was repeated four times with similar results. See also Table S2 for complete statistical
617 analysis results. **(B)** Transgenic seedlings described in (A) were treated with 100µM BTH overnight
618 (o/n). Total protein samples were resolved by PAGE and analysed by IB using anti-PR1 antibodies.
619 Equal loading is shown by CBB staining. The experiment was repeated with similar results. **(C)**
620 Infection assays with the virulent bacterial pathogen *Pseudomonas syringae* pv. *tomato* DC3000 (*Pst*)
621 empty vector. Six week-old plants were spray inoculated with a bacterial suspension of $5x10^8$
622 c.f.u./mL and analysed 0 and 3 days after inoculation. Data shown as mean +/- S.D. (n = 5). Letters
623 indicate statistically significant differences between c.f.u. in different lines three days after
624 inoculation (dai, One-Way ANOVA and Tukey post hoc test, $p < 0.05$). Similar results were obtained
625 in three independent experiments. **(D)** Infection assays with the avirulent bacterial pathogen
626 *Pseudomonas syringae* pv. *tomato* DC3000 *AvrRPS4*. Six week-old plants were syringe-infiltrated with
627 a bacterial suspension $O.D._{600}$ 0.001 and analysed 0 and 3 days after inoculation. Data shown as mean
628 +/- S.D. (n = 5). Letters indicate statistically significant differences (One-Way ANOVA and Tukey post
629 hoc test, $p < 0.05$).
630
631 **Figure 7. Working model for the regulation of Exo70B2 function by phosphorylation.**
632 Exo70B2 cycles between PM and the TGN under basal conditions, and upon BTH treatment, its
633 transport into the vacuole by autophagy is increased. Phosphorylated Exo70B2 is autophagocytosed
634 by interacting with ATG8.

635 ## Literature Cited

636 **Angelos, E., Ruberti, C., Kim, S.J., and Brandizzi, F.** (2017). Maintaining the factory: the roles of the
637 unfolded protein response in cellular homeostasis in plants. Plant J **90,** 671-682.
638 **Bethke, G., Pecher, P., Eschen-Lippold, L., Tsuda, K., Katagiri, F., Glazebrook, J., Scheel, D., and Lee,**
639 **J.** (2012). Activation of the Arabidopsis thaliana mitogen-activated protein kinase MPK11 by
640 the flagellin-derived elicitor peptide, flg22. Mol Plant Microbe Interact **25,** 471-480.
641 **Bodemann, B.O., Orvedahl, A., Cheng, T., Ram, R.R., Ou, Y.H., Formstecher, E., Maiti, M., Hazelett,**
642 **C.C., Wauson, E.M., Balakireva, M., Camonis, J.H., Yeaman, C., Levine, B., and White, M.A.**
643 (2011). RalB and the exocyst mediate the cellular starvation response by direct activation of
644 autophagosome assembly. Cell **144,** 253-267.
645 **Chien, Y., Kim, S., Bumeister, R., Loo, Y.M., Kwon, S.W., Johnson, C.L., Balakireva, M.G., Romeo, Y.,**
646 **Kopelovich, L., Gale, M., Jr., Yeaman, C., Camonis, J.H., Zhao, Y., and White, M.A.** (2006).
647 RalB GTPase-mediated activation of the IkappaB family kinase TBK1 couples innate immune
648 signaling to tumor cell survival. Cell **127,** 157-170.
649 **Cole, R.A., Synek, L., Zarsky, V., and Fowler, J.E.** (2005). SEC8, a subunit of the putative Arabidopsis
650 exocyst complex, facilitates pollen germination and competitive pollen tube growth. Plant
651 Physiol **138,** 2005-2018.
652 **Cvrckova, F., and Zarsky, V.** (2013). Old AIMs of the exocyst: evidence for an ancestral association of
653 exocyst subunits with autophagy-associated Atg8 proteins. Plant Signal Behav **8,** e27099.
654 **Cvrckova, F., Grunt, M., Bezvoda, R., Hala, M., Kulich, I., Rawat, A., and Zarsky, V.** (2012). Evolution
655 of the Land Plant Exocyst Complexes. Front Plant Sci **3,** 159.
656 **Dormann, P., Kim, H., Ott, T., Schulze-Lefert, P., Trujillo, M., Wewer, V., and Huckelhoven, R.**
657 (2014). Cell-autonomous defense, re-organization and trafficking of membranes in plant-
658 microbe interactions. New Phytol **204,** 815-822.
659 **Fujisaki, K., Abe, Y., Ito, A., Saitoh, H., Yoshida, K., Kanzaki, H., Kanzaki, E., Utsushi, H., Yamashita,**
660 **T., Kamoun, S., and Terauchi, R.** (2015). Rice Exo70 interacts with a fungal effector, AVR-Pii,
661 and is required for AVR-Pii-triggered immunity. Plant J **83,** 875-887.
662 **Furlan, G., Nakagami, H., Eschen-Lippold, L., Jiang, X., Majovsky, P., Kowarschik, K., Hoehenwarter,**
663 **W., Lee, J., and Trujillo, M.** (2017). Changes in PUB22 Ubiquitination Modes Triggered by
664 MITOGEN-ACTIVATED PROTEIN KINASE3 Dampen the Immune Response. The Plant Cell **29,**
665 726-745.
666 **Grefen, C., Donald, N., Hashimoto, K., Kudla, J., Schumacher, K., and Blatt, M.R.** (2010). A ubiquitin-
667 10 promoter-based vector set for fluorescent protein tagging facilitates temporal stability
668 and native protein distribution in transient and stable expression studies. Plant J. **64,** 355-
669 365.
670 **Grootjans, J., Kaser, A., Kaufman, R.J., and Blumberg, R.S.** (2016). The unfolded protein response in
671 immunity and inflammation. Nat Rev Immunol **16,** 469-484.
672 **Gu, Y., Zavaliev, R., and Dong, X.** (2017). Membrane Trafficking in Plant Immunity. Mol Plant **10,**
673 1026-1034.
674 **He, B., Xi, F., Zhang, X., Zhang, J., and Guo, W.** (2007a). Exo70 interacts with phospholipids and
675 mediates the targeting of the exocyst to the plasma membrane. EMBO J **26,** 4053-4065.
676 **He, P., Shan, L., and Sheen, J.** (2007b). The use of protoplasts to study innate immune responses.
677 Methods Mol Biol **354,** 1-9.
678 **Hofius, D., Schultz-Larsen, T., Joensen, J., Tsitsigiannis, D.I., Petersen, N.H., Mattsson, O.,**
679 **Jorgensen, L.B., Jones, J.D., Mundy, J., and Petersen, M.** (2009). Autophagic components
680 contribute to hypersensitive cell death in Arabidopsis. Cell **137,** 773-783.
681 **Honkanen, S., and Dolan, L.** (2016). Growth regulation in tip-growing cells that develop on the
682 epidermis. Curr Opin Plant Biol **34,** 77-83.
683 **Ichimura, Y., Kirisako, T., Takao, T., Satomi, Y., Shimonishi, Y., Ishihara, N., Mizushima, N., Tanida,**
684 **I., Kominami, E., Ohsumi, M., Noda, T., and Ohsumi, Y.** (2000). A ubiquitin-like system
685 mediates protein lipidation. Nature **408,** 488-492.

686 **Ishikawa, H., Ma, Z., and Barber, G.N.** (2009). STING regulates intracellular DNA-mediated, type I
687 interferon-dependent innate immunity. Nature **461,** 788-792.
688 **Jones, J.D., and Dangl, J.L.** (2006). The plant immune system. Nature **444,** 323-329.
689 **Kalde, M., Nuhse, T.S., Findlay, K., and Peck, S.C.** (2007). The syntaxin SYP132 contributes to plant
690 resistance against bacteria and secretion of pathogenesis-related protein 1. Proc Natl Acad
691 Sci U S A **104,** 11850-11855.
692 **Kalmbach, L., Hematy, K., De Bellis, D., Barberon, M., Fujita, S., Ursache, R., Daraspe, J., and**
693 **Geldner, N.** (2017). Transient cell-specific EXO70A1 activity in the CASP domain and
694 Casparian strip localization. Nat Plants **3,** 17058.
695 **Kirkin, V., Lamark, T., Sou, Y.S., Bjorkoy, G., Nunn, J.L., Bruun, J.A., Shvets, E., McEwan, D.G.,**
696 **Clausen, T.H., Wild, P., Bilusic, I., Theurillat, J.P., Overvatn, A., Ishii, T., Elazar, Z., Komatsu,**
697 **M., Dikic, I., and Johansen, T.** (2009). A role for NBR1 in autophagosomal degradation of
698 ubiquitinated substrates. Mol Cell **33,** 505-516.
699 **Kong, L., Cheng, J., Zhu, Y., Ding, Y., Meng, J., Chen, Z., Xie, Q., Guo, Y., Li, J., Yang, S., and Gong, Z.**
700 (2015). Degradation of the ABA co-receptor ABI1 by PUB12/13 U-box E3 ligases. Nat
701 Commun **6,** 8630.
702 **Kulich, I., Pecenkova, T., Sekeres, J., Smetana, O., Fendrych, M., Foissner, I., Hoftberger, M., and**
703 **Zarsky, V.** (2013). Arabidopsis exocyst subcomplex containing subunit EXO70B1 is involved in
704 autophagy-related transport to the vacuole. Traffic (Copenhagen, Denmark) **14,** 1155-1165.
705 **Lassowskat, I., Bottcher, C., Eschen-Lippold, L., Scheel, D., and Lee, J.** (2014). Sustained mitogen-
706 activated protein kinase activation reprograms defense metabolism and phosphoprotein
707 profile in Arabidopsis thaliana. Front Plant Sci **5,** 554.
708 **Lee, J., Rudd, J.J., Macioszek, V.K., and Scheel, D.** (2004). Dynamic changes in the localization of
709 MAPK cascade components controlling pathogenesis-related (PR) gene expression during
710 innate immunity in parsley. J. Biol. Chem. **279,** 22440-22448.
711 **Lee, J., Eschen-Lippold, L., Lassowskat, I., Bottcher, C., and Scheel, D.** (2015). Cellular
712 reprogramming through mitogen-activated protein kinases. Front Plant Sci **6,** 940.
713 **Leitner, J., Petrasek, J., Tomanov, K., Retzer, K., Parezova, M., Korbei, B., Bachmair, A., Zazimalova,**
714 **E., and Luschnig, C.** (2012). Lysine63-linked ubiquitylation of PIN2 auxin carrier protein
715 governs hormonally controlled adaptation of Arabidopsis root growth. Proc Natl Acad Sci U S
716 A **109,** 8322-8327.
717 **Li, S., van Os, G.M., Ren, S., Yu, D., Ketelaar, T., Emons, A.M., and Liu, C.M.** (2010). Expression and
718 functional analyses of EXO70 genes in Arabidopsis implicate their roles in regulating cell type-
719 specific exocytosis. Plant Physiol **154,** 1819-1830.
720 **Liao, D., Cao, Y., Sun, X., Espinoza, C., Nguyen, C.T., Liang, Y., and Stacey, G.** (2017). Arabidopsis E3
721 ubiquitin ligase PLANT U-BOX13 (PUB13) regulates chitin receptor LYSIN MOTIF RECEPTOR
722 KINASE5 (LYK5) protein abundance. New Phytol.
723 **Lin, Y., Ding, Y., Wang, J., Shen, J., Kung, C.H., Zhuang, X., Cui, Y., Yin, Z., Xia, Y., Lin, H., Robinson,**
724 **D.G., and Jiang, L.** (2015). Exocyst-Positive Organelles and Autophagosomes Are Distinct
725 Organelles in Plants. Plant Physiol **169,** 1917-1932.
726 **Liu, J., Zuo, X., Yue, P., and Guo, W.** (2007). Phosphatidylinositol 4,5-bisphosphate mediates the
727 targeting of the exocyst to the plasma membrane for exocytosis in mammalian cells. Mol Biol
728 Cell **18,** 4483-4492.
729 **Lu, D., Lin, W., Gao, X., Wu, S., Cheng, C., Avila, J., Heese, A., Devarenne, T.P., He, P., and Shan, L.**
730 (2011). Direct ubiquitination of pattern recognition receptor FLS2 attenuates plant innate
731 immunity. Science **332,** 1439-1442.
732 **Mao, H., Nakamura, M., Viotti, C., and Grebe, M.** (2016). A Framework for Lateral Membrane
733 Trafficking and Polar Tethering of the PEN3 ATP-Binding Cassette Transporter. Plant Physiol
734 **172,** 2245-2260.
735 **Marshall, R.S., Li, F., Gemperline, D.C., Book, A.J., and Vierstra, R.D.** (2015). Autophagic Degradation
736 of the 26S Proteasome Is Mediated by the Dual ATG8/Ubiquitin Receptor RPN10 in
737 Arabidopsis. Mol. Cell **58,** 1053-1066.

738 **Martins, S., Dohmann, E.M., Cayrel, A., Johnson, A., Fischer, W., Pojer, F., Satiat-Jeunemaitre, B.,**
739 **Jaillais, Y., Chory, J., Geldner, N., and Vert, G.** (2015). Internalization and vacuolar targeting
740 of the brassinosteroid hormone receptor BRI1 are regulated by ubiquitination. Nat Commun
741 **6,** 6151.
742 **McCloy, R.A., Rogers, S., Caldon, C.E., Lorca, T., Castro, A., and Burgess, A.** (2014). Partial inhibition
743 of Cdk1 in G 2 phase overrides the SAC and decouples mitotic events. Cell Cycle **13,** 1400-
744 1412.
745 **Mei, K., Li, Y., Wang, S., Shao, G., Wang, J., Ding, Y., Luo, G., Yue, P., Liu, J.J., Wang, X., Dong, M.Q.,**
746 **Wang, H.W., and Guo, W.** (2018). Cryo-EM structure of the exocyst complex. Nature
747 structural & molecular biology.
748 **Moore, B.A., Robinson, H.H., and Xu, Z.** (2007). The crystal structure of mouse Exo70 reveals unique
749 features of the mammalian exocyst. J Mol Biol **371,** 410-421.
750 **Nagashima, Y., Iwata, Y., Ashida, M., Mishiba, K., and Koizumi, N.** (2014). Exogenous salicylic acid
751 activates two signaling arms of the unfolded protein response in Arabidopsis. Plant & cell
752 physiology **55,** 1772-1778.
753 **Noda, N.N., Ohsumi, Y., and Inagaki, F.** (2010). Atg8-family interacting motif crucial for selective
754 autophagy. FEBS Lett **584,** 1379-1385.
755 **Novick, P., Field, C., and Schekman, R.** (1980). Identification of 23 complementation groups required
756 for post-translational events in the yeast secretory pathway. Cell **21,** 205-215.
757 **Ostertag, M., Stammler, J., Douchkov, D., Eichmann, R., and Huckelhoven, R.** (2013). The conserved
758 oligomeric Golgi complex is involved in penetration resistance of barley to the barley
759 powdery mildew fungus. Mol Plant Pathol **14,** 230-240.
760 **Pecenkova, T., Hala, M., Kulich, I., Kocourkova, D., Drdova, E., Fendrych, M., Toupalova, H., and**
761 **Zarsky, V.** (2011). The role for the exocyst complex subunits Exo70B2 and Exo70H1 in the
762 plant-pathogen interaction. J Exp Bot **62,** 2107-2116.
763 **Pleskot, R., Cwiklik, L., Jungwirth, P., Zarsky, V., and Potocky, M.** (2015). Membrane targeting of the
764 yeast exocyst complex. Biochim Biophys Acta **1848,** 1481-1489.
765 **Ren, J., and Guo, W.** (2012). ERK1/2 regulate exocytosis through direct phosphorylation of the
766 exocyst component Exo70. Dev Cell **22,** 967-978.
767 **Safavian, D., and Goring, D.R.** (2013). Secretory activity is rapidly induced in stigmatic papillae by
768 compatible pollen, but inhibited for self-incompatible pollen in the Brassicaceae. PLoS One **8,**
769 e84286.
770 **Safavian, D., Zayed, Y., Indriolo, E., Chapman, L., Ahmed, A., and Goring, D.R.** (2015). RNA Silencing
771 of Exocyst Genes in the Stigma Impairs the Acceptance of Compatible Pollen in Arabidopsis.
772 Plant Physiol **169,** 2526-2538.
773 **Samuel, M.A., Chong, Y.T., Haasen, K.E., Aldea-Brydges, M.G., Stone, S.L., and Goring, D.R.** (2009).
774 Cellular pathways regulating responses to compatible and self-incompatible pollen in
775 Brassica and Arabidopsis stigmas intersect at Exo70A1, a putative component of the exocyst
776 complex. Plant Cell **21,** 2655-2671.
777 **Stegmann, M., Anderson, R.G., Westphal, L., Rosahl, S., McDowell, J.M., and Trujillo, M.** (2013). The
778 exocyst subunit Exo70B1 is involved in the immune response of Arabidopsis thaliana to
779 different pathogens and cell death. Plant Signal Behav **8,** e27421.
780 **Stegmann, M., Anderson, R.G., Ichimura, K., Pecenkova, T., Reuter, P., Zarsky, V., McDowell, J.M.,**
781 **Shirasu, K., and Trujillo, M.** (2012). The ubiquitin ligase PUB22 targets a subunit of the
782 exocyst complex required for PAMP-triggered responses in Arabidopsis. Plant Cell **24,** 4703-
783 4716.
784 **Svenning, S., Lamark, T., Krause, K., and Johansen, T.** (2011). Plant NBR1 is a selective autophagy
785 substrate and a functional hybrid of the mammalian autophagic adapters NBR1 and
786 p62/SQSTM1. Autophagy **7,** 993-1010.
787 **Tateda, C., Zhang, Z., Shrestha, J., Jelenska, J., Chinchilla, D., and Greenberg, J.T.** (2014). Salicylic
788 acid regulates Arabidopsis microbial pattern receptor kinase levels and signaling. Plant Cell
789 **26,** 4171-4187.

790 **Tzfadia, O., and Galili, G.** (2013). The Arabidopsis exocyst subcomplex subunits involved in a golgi-
791 independent transport into the vacuole possess consensus autophagy-associated atg8
792 interacting motifs. Plant Signal Behav **8,** doi: 10 4161/psb 26732.
793 **Vlot, A.C., Dempsey, D.A., and Klessig, D.F.** (2009). Salicylic Acid, a multifaceted hormone to combat
794 disease. Annu. Rev. Phytopathol. **47,** 177-206.
795 **Wang, D., Weaver, N.D., Kesarwani, M., and Dong, X.** (2005). Induction of protein secretory
796 pathway is required for systemic acquired resistance. Science **308,** 1036-1040.
797 **Wen, T.J., Hochholdinger, F., Sauer, M., Bruce, W., and Schnable, P.S.** (2005). The roothairless1
798 gene of maize encodes a homolog of sec3, which is involved in polar exocytosis. Plant Physiol
799 **138,** 1637-1643.
800 **Wu, B., and Guo, W.** (2015). The Exocyst at a Glance. J Cell Sci **128,** 2957-2964.
801 **Yoshimoto, K., Jikumaru, Y., Kamiya, Y., Kusano, M., Consonni, C., Panstruga, R., Ohsumi, Y., and**
802 **Shirasu, K.** (2009). Autophagy negatively regulates cell death by controlling NPR1-dependent
803 salicylic acid signaling during senescence and the innate immune response in Arabidopsis.
804 The Plant cell **21,** 2914-2927.
805 **Zhang, C., Brown, M.Q., van de Ven, W., Zhang, Z.M., Wu, B., Young, M.C., Synek, L., Borchardt, D.,**
806 **Harrison, R., Pan, S., Luo, N., Huang, Y.M., Ghang, Y.J., Ung, N., Li, R., Isley, J., Morikis, D.,**
807 **Song, J., Guo, W., Hooley, R.J., Chang, C.E., Yang, Z., Zarsky, V., Muday, G.K., Hicks, G.R.,**
808 **and Raikhel, N.V.** (2016). Endosidin2 targets conserved exocyst complex subunit EXO70 to
809 inhibit exocytosis. Proc Natl Acad Sci U S A **113,** E41-50.
810 **Zhang, L., Chen, H., Brandizzi, F., Verchot, J., and Wang, A.** (2015). The UPR branch IRE1-bZIP60 in
811 plants plays an essential role in viral infection and is complementary to the only UPR
812 pathway in yeast. PLoS Genet **11,** e1005164.
813 **Zhao, T., Rui, L., Li, J., Nishimura, M.T., Vogel, J.P., Liu, N., Liu, S., Zhao, Y., Dangl, J.L., and Tang, D.**
814 (2015). A truncated NLR protein, TIR-NBS2, is required for activated defense responses in the
815 exo70B1 mutant. PLoS Genet **11,** e1004945.
816 **Zhao, Y., Liu, J., Yang, C., Capraro, B.R., Baumgart, T., Bradley, R.P., Ramakrishnan, N., Xu, X.,**
817 **Radhakrishnan, R., Svitkina, T., and Guo, W.** (2013). Exo70 generates membrane curvature
818 for morphogenesis and cell migration. Dev Cell **26,** 266-278.
819 **Zhou, J., Liu, D., Wang, P., Ma, X., Lin, W., Chen, S., Mishev, K., Lu, D., Kumar, R., Vanhoutte, I.,**
820 **Meng, X., He, P., Russinova, E., and Shan, L.** (2018). Regulation of Arabidopsis
821 brassinosteroid receptor BRI1 endocytosis and degradation by plant U-box PUB12/PUB13-
822 mediated ubiquitination. Proceedings of the National Academy of Sciences.
823 **Zipfel, C., Robatzek, S., Navarro, L., Oakeley, E.J., Jones, J.D., Felix, G., and Boller, T.** (2004).
824 Bacterial disease resistance in Arabidopsis through flagellin perception. Nature **428,** 764-767.

825

826 Figure 1

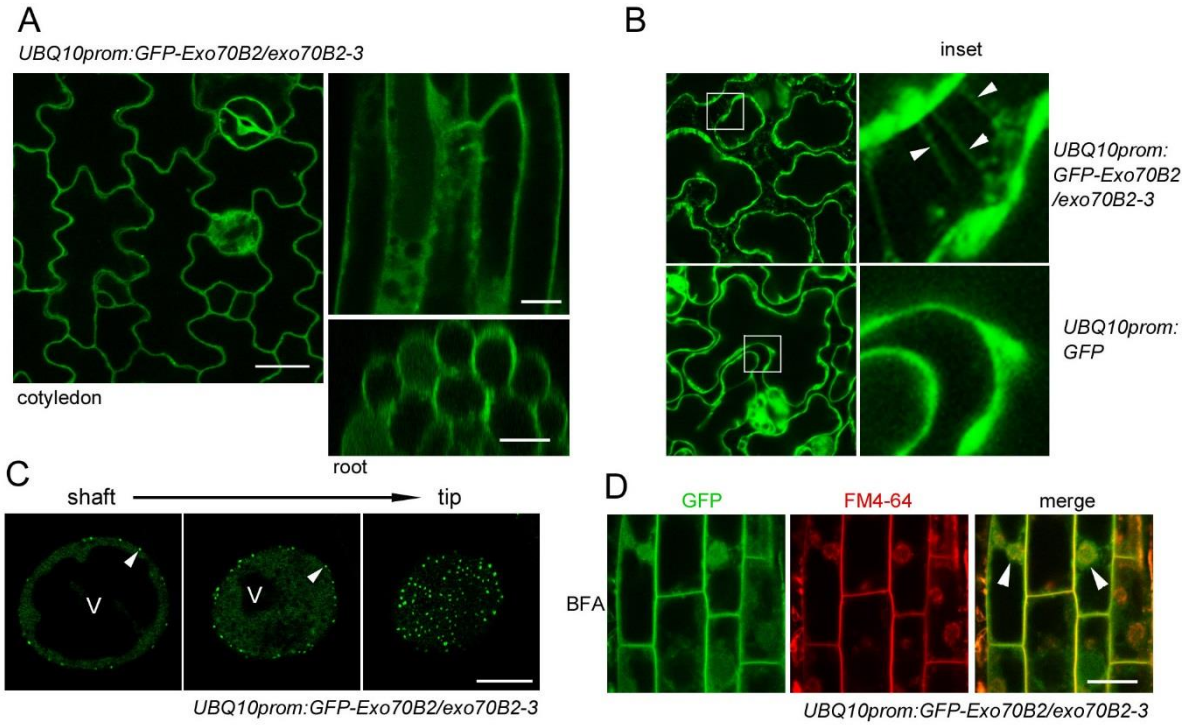

827

828 Figure 2

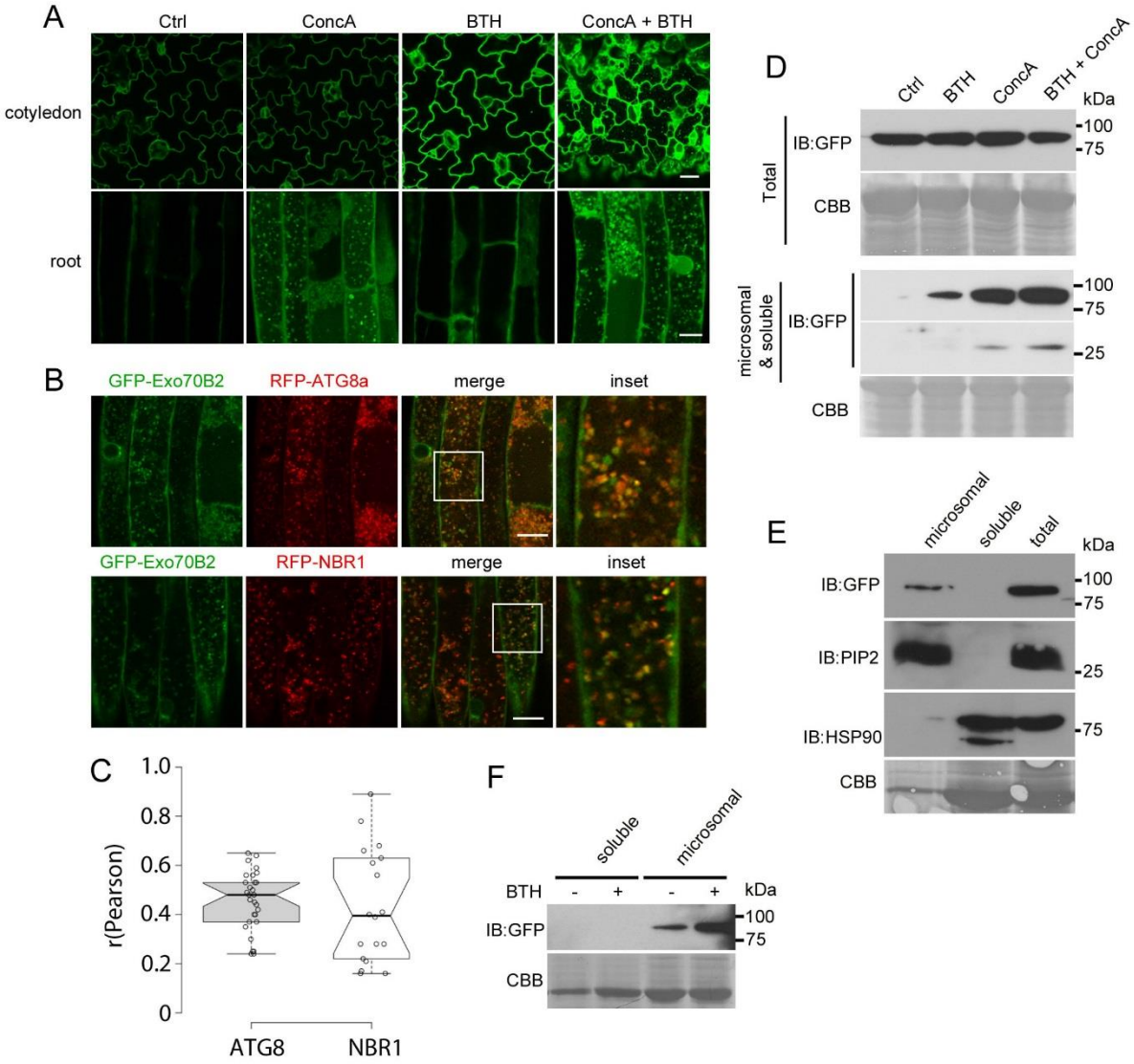

829

830 Figure 3

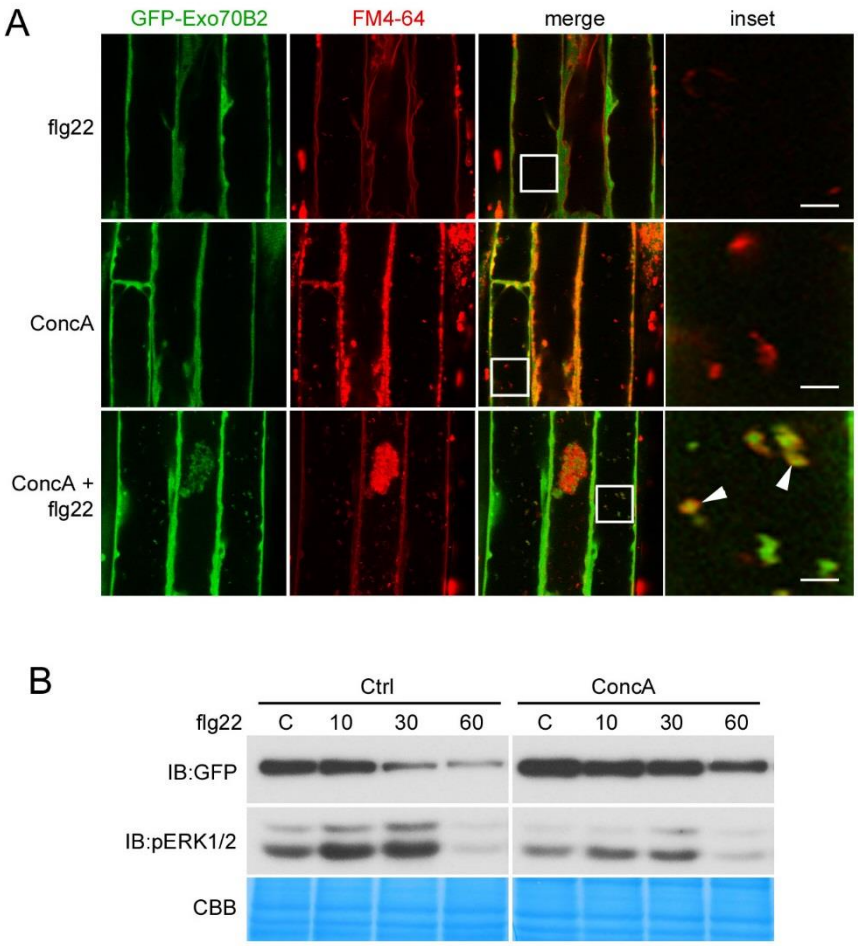

831

832 Figure 4

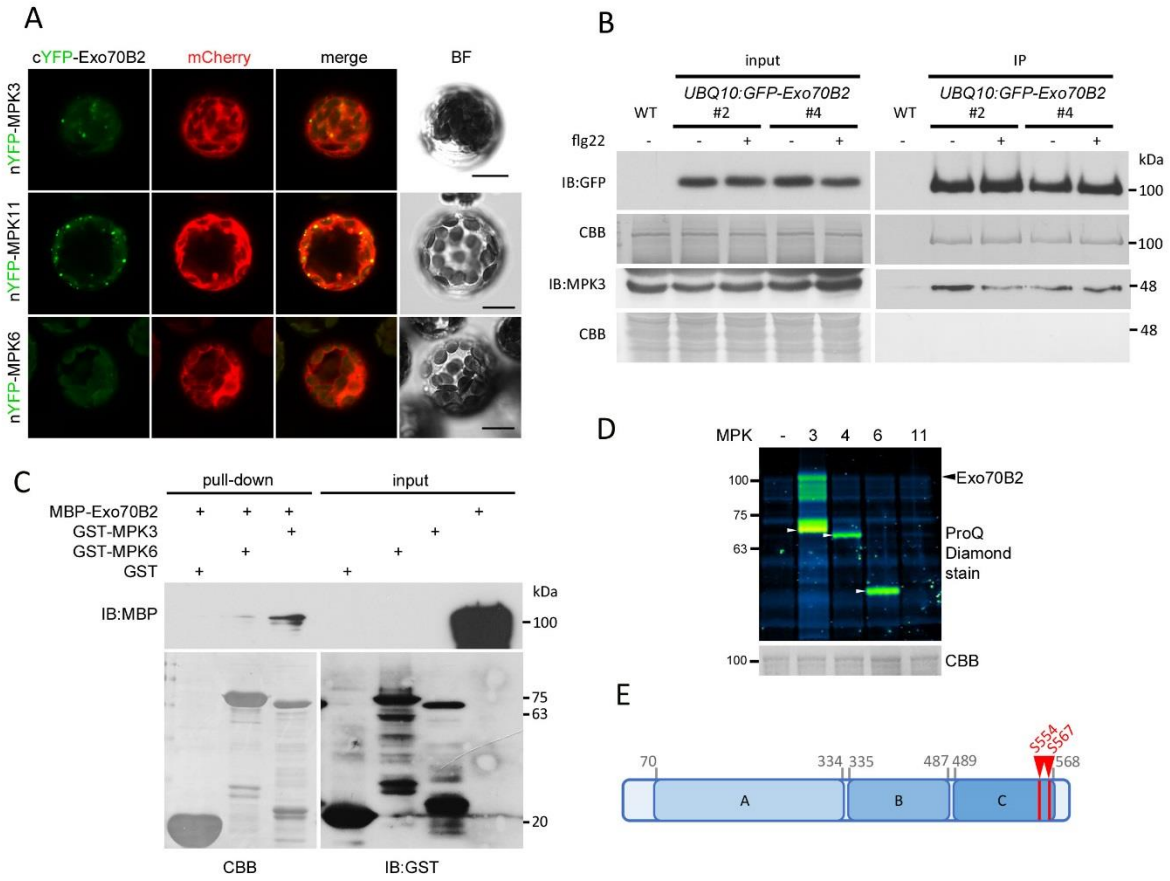

833

834 Figure 5

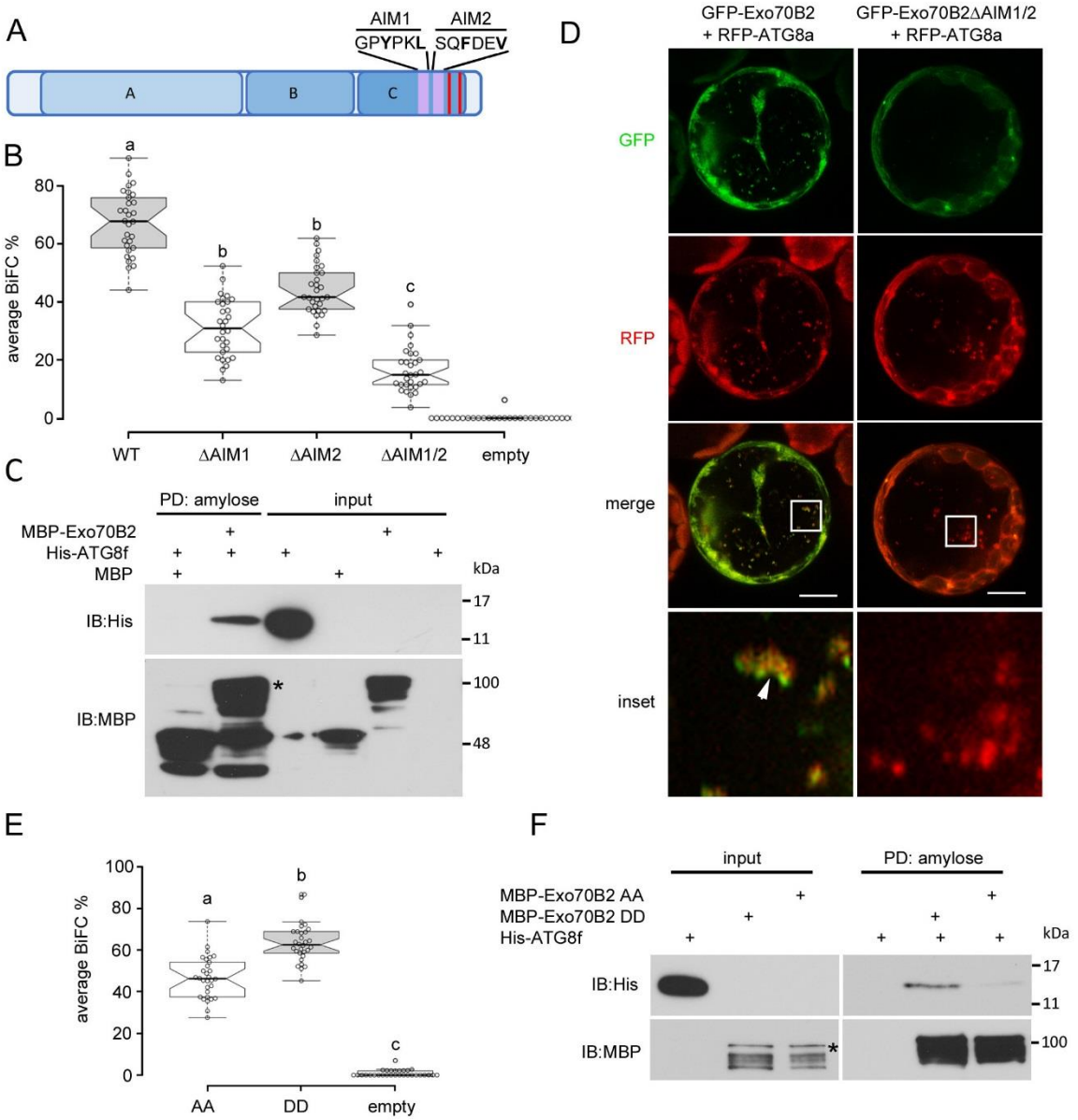

835

836 Figure 6

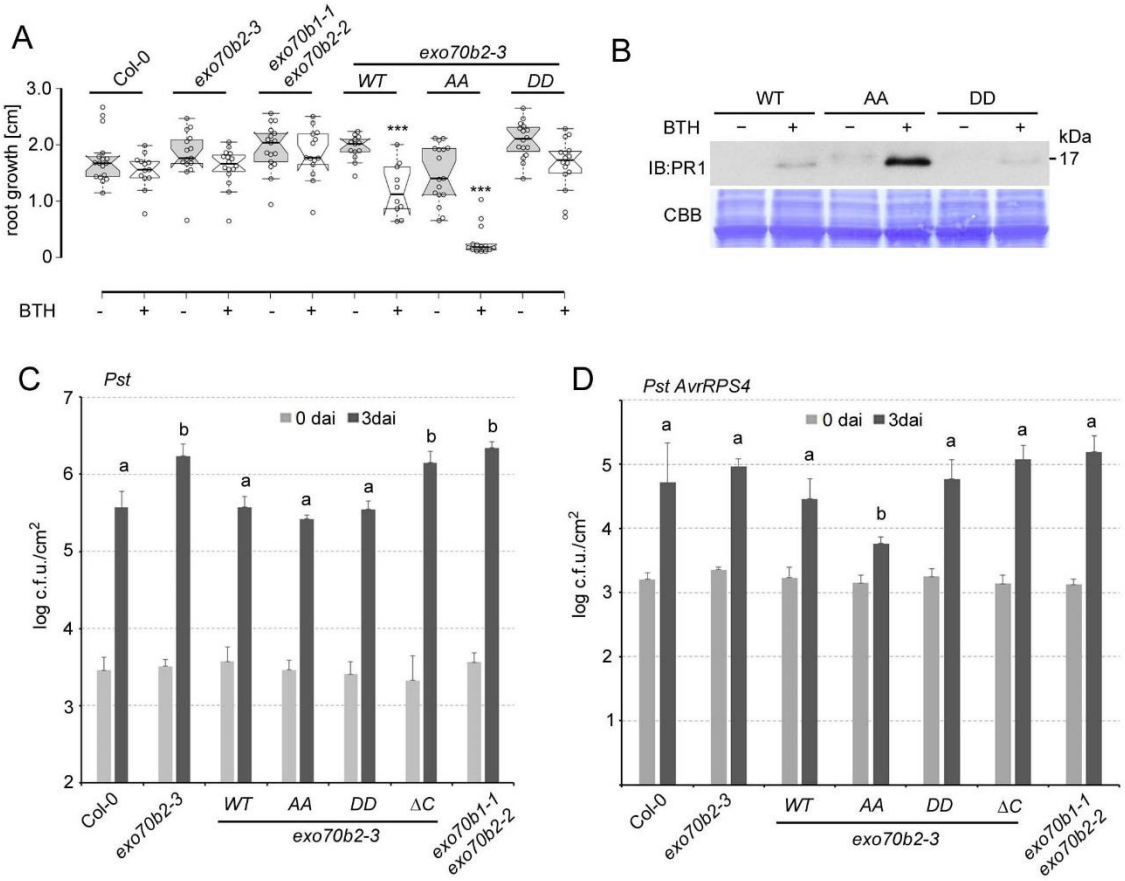

837

838 Figure 7

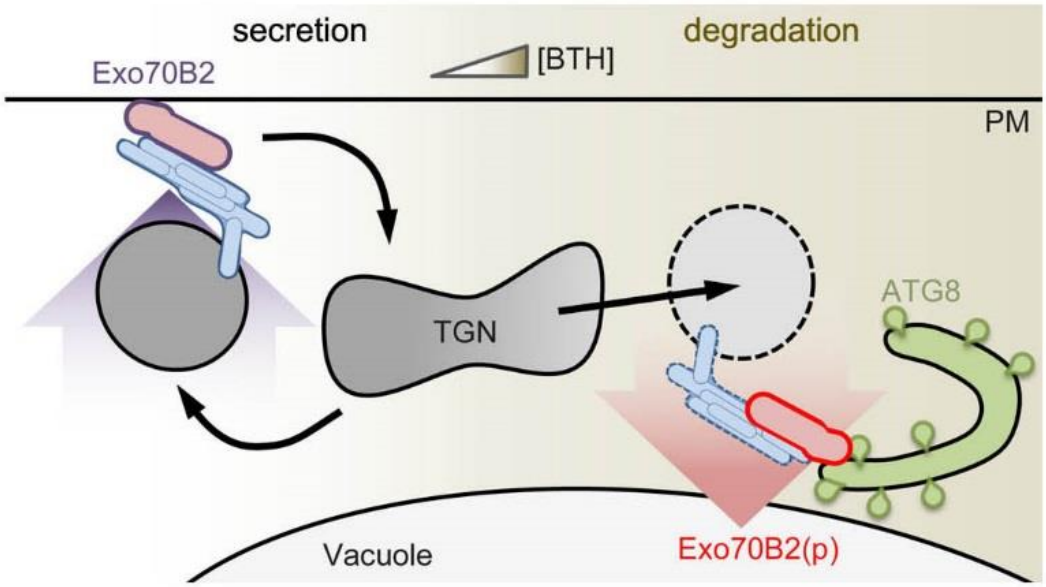

839